Spanwise Streaky Structure and Macroturbulence in Open-channel Flows*

By

Hiroji NAKAGAWA**, Iehisa NEZU** and Akihiro TOMINAGA**

(Received September 29, 1980)

Abstract

In order to reveal the interrelation between the bursting phenomenon occurring originally in the wall region and the macroturbulence such as kolk-boils and the cellular secondary current, which are observed in the outer region of an actual river, the present study has examined the spanwise spatial structures of open-channel flows with and without the cellular secondary current which was created artificially. A new conditional averaging technique, whereby the signals of a sampling probe are weight-averaged by the sorted instantaneous Reynolds-stress signals of a detection probe, has been used to evaluate the mean spanwise streaky spacings throughout the flow depth. The direct effect of the cellular secondary current on the bursting motion was not recognized. It was suggested that the coherent structures of an open-channel flow would indicate the double-structure of turbulence, in which both the bursting and macroturbulence coexist self-consistently.

1. Introduction

The boundary layer, pipe and open-channel flows are classified as the wall turbulence, which is characterized by a strong shear stress near the wall. Modern turbulence research[1] has revealed that the wall turbulence field consists of both inner and outer layers. The inner layer is characterized by the viscous stress represented by the kinematic viscosity ν, and also the Reynolds stress represented by the friction velocity U_*. The outer layer is the region farther from the wall, in which the strong Reynolds shear stress is fairly relaxed, and the effects of the outer (mainstream) boundary conditions appear. An open-channel flow field can also be divided into the wall region (inner layer) and the outer region, as shown in Fig. 1. The wall region is controlled by the inner variables of ν/U_*, while the outer region is controlled by the outer variables of the flow depth h and the free-surface velocity

* Main part of the present paper was lectured at the ICHMT/IUTAM Symposium on Heat and Mass Transfer and the Structure of Turbulence, which was held in Dubrovnik, October 6–10, 1980[39].

** Department of Civil Engineering

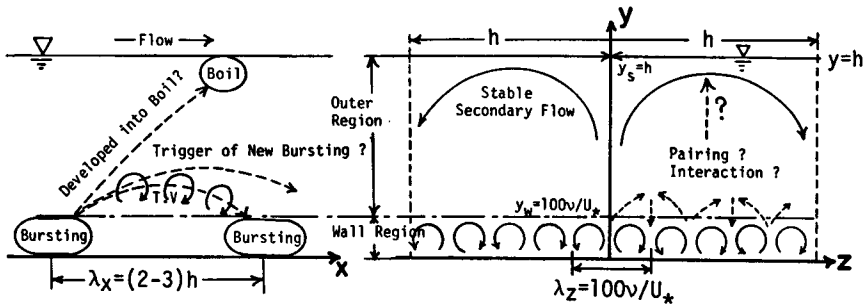

Fig. 1. Illustration of coherent structures in an open-channel flow.

U_{max}. Only in the outer region does the effect of the free surface, peculiar to the open channel flow, appear.[2)]

We consider a fully developed, two-dimensional and normal open-channel flow in Fig. 1. The x coordinate is aligned with the mainstream velocity. y is the vertical coordinate to the wall, and z is in a spanwise direction. The velocity fluctuations in the x, y and z directions are u, v and w, and also their r.m.s. values (i.e. the turbulence intensities) are u', v' and w', respectively. The edge y_w of the wall region is given by $y_w=100\nu/U_*$. When the Reynolds number $R_*\equiv hU_*/\nu$ is sufficiently large, $y_w/h=100/R_*$ becomes very small, and thus the flow field is almost occupied by the outer region (e.g. Nezu 1977[2)]). The large-scale turbulence in an actual river, observed hitherto by many river engineers, corresponds to the fluid motions in the outer region, which were generally termed 'macroturbulence' by Matthes (1947)[3)]. He proposed the noticeable suggestions that there might exist a strong upward and intermittent current, like a tornado, near the river bed. (He called it 'kolk'.) Its vortex developed up to the free surface and then became a so-called 'boil', which was observed as a vortex-ring-like swollen water surface of the river. The hydraulic behaviours of boils were then examined through an aerial photo-survey by Kinoshita (1967)[4)] and Coleman (1969)[5)], as described in Table 1. They found that a boil formed a low-speed zone and, at both spanwise sides with the spacing of twice the flow depth h, high-speed zones were formed, as shown in Fig. 1. They also suggested that there might exist cellular secondary currents in a straight river which had a pair of counter-rotating streamwise vortices with a vortex diameter of about h. (*See Figs. 1 and 2.*) Such a macroturbulence in the outer region has been regarded as very important phenomena in hydraulic engineering, because it might be closely related to the formation of various bed configurations. Also, it might cause sediment transportation and three-dimensional flow patterns in an actual river. However, the origin of the macroturbulence and its physical mechanism are quite unknown at present.

Table 1. Subdivision of wall turbulence field and its typical research.

	Wall Region ($y^+ \leq 100$)	Outer Region ($y^+ \geq 100$)
Phenomena	Bursting Process of ejections and sweeps appears in common in Boundary Layer, Pipe and Open-channel Flows.	Bulges Motion (Boundary Layer) Core Motion (Pipe) Kolk-Boil and Cellular Secondary Currents (Open-channel)
Flow Visualization Hydrogen-bubble, Aerial Photosurvey Dye Tracer etc.	Kline et al. (1967, 71, 74, 75): B.L. Flow Brodkey et al. (1969, 73, 78): Pipe Flow Grass (1971), Nakagawa & Nezu (1977): Open-channel Flow	Bulges = Many studies (e.g. Falco 1977) since 1950's (NACA) Boils = Observation of water surface of river (Matthes 1947, Kinoshita 1967, Coleman 1969, Jackson 1976, etc.)
Probe Measurements Hot-wires Hot-films Laser D.V.	Laufer et al. (1971) Eckelmann et al. (1974, 77, 79) Hanratty et al. (1974, 77) Nishioka et al. (1977)	Almost in viscous sublayer *Streaky Wall Structure*
Conditional Analysis	Willmarth et al. (1972, 73, 75) Blackwelder et al. (1972, 76, 78)	Up to the edge of boundary layer ($y \leq \delta$)
	Sabot et al. (1976)	Up to the center axis ($y \leq D/2$) of pip eflow
	Nakagawa & Nezu (1977, 78, 79, 80)	Up to the water surface ($y \leq h$) of open-channel

On the other hand, in the last decade, many flow visualization studies as well as probe measurements of wall turbulent shear flows have shown that the wall region is dominated by a sequence of events such as ejections and sweeps which has been termed the bursting phenomenon. This sequence of events is first noticed by the occurrence of low-speed streaks ($u<0$) in the streamwise direction. A part of these streaks lifts up away from the wall, i.e. $v>0$, and then breaks down in an ejection phase. This is followed by a sweep of high-speed fluid ($u>0$) that originates in the outer region and moves in a small angle toward the wall, i.e. $v<0$. Then, the most important feature of the bursting phenomenon is to be accompanied with most of the production of the turbulent energy and the Reynolds stress, i.e. $-uv>0$. Also, its occurrence is fairly random at one place or time, while a sequence of the bursting motions has a quasi-orderly process. For further details, Hinze (1975)[1], Laufer (1975)[6] and Willmarth (1975)[7] have written excellent reviews which describe the recent status of research on solid-wall turbulence, especially on the bursting phenomenon of boundary layers.

As shown in Table 1, a close interrelation between the inner and outer layers, i.e. between the bursting and bulge motions in the boundary layer, has been suggested through the visual observations and the hot-wire measurements by Laufer & Narayanan (1971)[8], Blackwelder & Kovasznay (1972)[9], Offen & Kline (1975)[10],

Falco (1977)[11], Brown & Thomas (1977)[12] and Praturi & Brodkey (1978)[13]. A close interrelation between the wall and free-surface regions, i.e. the bursting and boil phenomena in an open channel, has also been suggested by Grass (1971)[14], Jackson (1976)[15] and the authors (1978)[16]. Fig. 1 shows an illustration of the coherent structures in an open-channel flow, on the basis of previous visual observations. The most notable characteristics are: (1) The bursting period T_B and the streamwise spacing λ_x of the bursting motions in an open-channel flow are controlled by the outer variables of h and U_{max}, while its spanwise spacing λ_z is controlled by the inner variables of ν/U_* (Nakagawa & Nezu 1978[16]). (2) The boil or cellular secondary current appears at a nearly fixed position on the free surface, and it is controlled by the outer variables (Kinoshita 1967[4], Jackson 1976[15]). From these visual results, the following essential and important questions arise.

(1) *Does a bursting motion grow into a transverse vorter (T.V.) in the outer region, and in turn does its vortex generate a new bursting motion at the downstream in the wall region?*

(2) *Does a strong bursting motion develop up to the free surface and then become a boil or cellular secondary current?*

Therefore, an investigation of the space-time structure of the bursting phenomenon, which occurs originally near the buffer layer and then shows a coherent and organized behaviour during its convection process, will contribute not only to the elucidation of these questions, but also to the refinement of the physical description of the bursting phenomenon.

In the light of the above, the authors have recently (1980)[17] investigated the structure of space-time correlations of bursting events, such as ejections and sweeps, in the x-y center plane of a smooth open-channel flow (*See Fig. 1*), by the conditional sampling of the instantaneous Reynolds-stress signals measured simultaneously at two different points. One probe was fixed near the edge of the buffer layer and used as a detection probe of the bursting motions, and the other probe was moved in both streamwise and vertical directions. The temporal and spatial scales of the ejection and sweep motions and their convective process were investigated in detail experimentally.*)

In the present study, the spanwise spatial structure in the y-z plane will be examined further, in order to reveal some interrelation between the high-and low-speed streaks of the bursting motions and the cellular secondary currents, as shown in Fig. 1.

*) A more detailed discussion of these results will be published soon in Journal of Fluid Mechanics (1981)[40].

2. New Detection Scheme of Bursting Process and Conditional Average

Although the bursting phenomenon occurs fairly random at one place and time, a sequence of its bursting events has a quasi-orderly process. It seems, therefore, that significant information cannot be obtained by the conventional 'long-time' averaging technique, as pointed out by many researchers.[7),16-18)] Hence, a conditional sampling method which detects significant information from the fluctuating velocity signals has been experimented by the authors (1980).[17)]

In general, the conditional average of an arbitrary velocity signal $u(x_1, y_1, z_1, t+\tau)$ can be defined as follows:

$$\langle u\rangle(x_1, y_1, z_1, \tau) = \frac{\int_T u(x_1, y_1, z_1, t+\tau)\cdot I(x_0, y_0, z_0, t)dt}{\int_T I(x_0, y_0, z_0, t)dt} \tag{1}$$

where, $\int_T \cdots dt$ means $\lim_{T\to\infty} T^{-1}\int_0^T \cdots dt$. $I(x_0, y_0, z_0, t)$ is the detection function of the turbulence phenomenon in question which occurs at the point of (x_0, y_0, z_0, t). For example, the detection function I of the bulge phenomena in the boundary layer can be definitely given by the intermittency function.[9)]

However, the detection function I of the bursting phenomenon near the wall is not sufficiently established yet, although several detection functions have been proposed by Lu & Willmarth (1973)[19)], Brodkey et al. (1974)[20)], Blackwelder & Kaplan (1976)[21)], Wallace et al. (1977)[22)], Nakagawa & Nezu (1978)[16)] and others. As already pointed out in our previous paper (1978)[16)], the instantaneous Reynolds-stress signals $u(t)v(t)$ can be reasonably used as discriminating information, since they are directly related to the bursting phenomenon or the mechanism of turbulence production. Then, because the ejection and sweep events contribute mostly to the turbulence production, the sorting functions of ejection $I_e(t)$, and sweep $I_s(t)$, are defined here, respectively, as follows:[23)]

$$I_e(t) = \begin{cases} 1 & \text{for } u(t)<0 \text{ and } v(t)>0 \\ 0 & \text{otherwise} \end{cases}, \quad I_s(t) = \begin{cases} 1 & \text{for } u(t)>0 \text{ and } v(t)<0 \\ 0 & \text{otherwise} \end{cases} \tag{2}$$

Unfortunately, $I_e(t)$ or $I_s(t)$ should not be regarded directly as the detection function $I(t)$ for the bursting motions, because the ejection and sweep events in the sorted Reynolds-stress signals still contain interaction-like motions.[16)] Therefore, Lu & Willmarth (1973),[19)] Sabot & Comte-Bellot (1976)[24)] and the authors (1977-78-79)[23),16),25)] introduced a threshold level H in the Reynolds stress signals, and

assumed that the bursting motions occurred only when $|u(t)\cdot v(t)| \geq H$. However, the determination of the threshold level H is more or less arbitrary, because stationary values of the conditionally averaged patterns against the variation of H do not exist definitely (Nakagawa & Nezu 1978[16]). Moreover, especially in the water flow measurements, such a threshold method has the following shortcomings. Since the bursting period T_B is of the order of one second in ordinary laboratory experiments (*See Fig. 20.*), continuous velocity signals longer than 500 seconds are needed in order to obtain an accurate ensemble average by the threshold method. However, accurate signal data cannot be expected by long-time measurements, because the sensitivity of hot-film anemometers will decay by being coated with the impurities in water flow.

In order to overcome the above shortcomings of the threshold method, the authors have recently (1980)[17] proposed a new detection function weighted by the instantaneous Reynolds-stress signal itself, i.e. $I(t) \equiv u(t)v(t)\cdot I_e(t)$ for the ejection phase and $I(t) \equiv u(t)v(t)\cdot I_s(t)$ for the sweep phase. Then, the conditional average of the space-time correlations of the ejection and sweep motions can be definitely given by, respectively,

$$\langle u\rangle_e(x_1, y_1, z_1, \tau) = \frac{\int_T u(x_1, y_1, z_1, t+\tau)\cdot\{u(t)v(t)I_e(t)\}_0 dt}{\int_T \{u(t)v(t)I_e(t)\}_0 dt} \tag{3}$$

$$\langle u\rangle_s(x_1, y_1, z_1, \tau) = \frac{\int_T u(x_1, y_1, z_1, t+\tau)\cdot\{u(t)v(t)I_s(t)\}_0 dt}{\int_T \{u(t)v(t)I_s(t)\}_0 dt} \tag{4}$$

where the suffix $\{\ \}_0$ denotes the position of the detection probe.

Eqs. (3) and (4) imply that the stronger instantaneous Reynolds-stress is more contributive to the average structure of the bursting phenomenon. Although the above method cannot detect each instantaneous bursting event separately, it is preferable to the threshold method. This is because the structure of bursting motions can be evaluated more objectively without introducing any arbitrary parameter. Also, the random components such as background turbulence are to be cancelled on averaging larger amounts of data.

The validity of Eqs. (3) and (4) was confirmed by the authors (1980)[17] through a comparison with the results obtained by previous threshold methods, e.g. the method of $|u(t)v(t)| \geq H$, the VITA-method of Blackwelder & Kaplan (1976)[21] and the pattern recognition of Wallace et al. (1977).[22]

3. Experimental Techniques and Data Procedures

3.1 Experimental Set-up

Three groups of experiments on a two-dimensional, fully developed and normal turbulent flow in a smooth open-channel, whose hydraulic conditions are described in Table 2, were conducted in a tilting flume 15 m long, 50 cm wide and 30 cm deep at the Hydraulics Laboratory in Civil Engineering, Kyoto University. This experimental set-up was the same as that previously used by the authors (1977-78-79-80),[23),16),25),17)]. A settling chamber and screens to prevent the occurrence of large-scale disturbances and the distortion of the main surface flow were set up at the entrance of the channel. Consequently, a fully developed turbulent shear flow was obtained at the test section 9.5 m downstream from the entrance.

Most previous research work on the bursting phenomenon has dealt with that over a smooth flat bed. The bursting phenomena over a rough bed, however are little known at present since the existence of the wall region itself becomes unclear, although a burst-like behaviour has been discovered even over a completely rough bed by Grass (1971)[14)] and Nakagawa & Nezu (1977).[23)] On the other hand, all of the macroturbulences in the outer region of a river (*See Table 1.*) were observed over rough flat beds or wavy sand beds. It is questionable whether they appear over a smooth flat bed. Thus, a reasonable device is needed by which a macro-

Table 2. Hydraulic conditions for the experiments.

Series of Experiments		Case R-1	Case R-2	Case R-3	Case R-4	Case R-5	Case R-6
Flow Conditions		Throughout Solid Bed		With Interval Injections		With Interval Roughness	
Flow depth	h (cm)	7.7	7.9	4.0	4.0	4.0	4.0
Discharge	Q (l/sec)	5.5	2.2	2.8	2.8	2.6	2.6
Free-surface velocity	U_{max} (cm/sec)	20.4	8.4	21.0	21.0	22.2	19.9
Mean velocity	U_m (cm/sec)	14.1	5.5	13.9	13.9	13.0	13.0
Friction velocity	U_* (cm/sec)	0.94	0.42	0.96	0.96	1.05	0.91
Injection velocity	v_0 (cm/sec)	0.0	0.0	0.47	0.53	0.0	0.0
Reynolds number	$R_e \equiv U_m h/\nu$ $R_* \equiv U_* h/\nu$	1.1×10^4 696.	0.42×10^4 318.	0.54×10^4 375.	0.54×10^4 376.	0.52×10^4 408.	0.52×10^4 358.
Froude number	$F_r \equiv U_m/\sqrt{gh}$	0.16	0.063	0.22	0.22	0.21	0.21
Water temperature	T_w (°C)	18.7	19.6	19.2	19.7	19.1	19.9
Roughness Element						5×5 mm	5×10 mm

turbulence such as cellular secondary currents is created artificially over a smooth flat bed. Therefore, in the present study, three kinds of experiments were carried out as follows.

Uniform flow over a smooth bed (Cases R-1 and R-2). This flow is the most fundamental one in open-channels, since the bed or wall is uniformly smooth, flat and solid. Two kinds of hydraulic conditions were set, as described in Table 2. Case R-1 had nearly the same hydraulic condition as in our previous experiments which examined the bursting structure in the *x-y* plane (Nakagawa et al. 1980[17]). The Reynolds number in Case R-2 was equal to about a half of that in Case R-1, and it then became easier to compare the results of Case R-2 with visual data.

Flow with 5 mm-slit injections with uniform spanwise spacings (Cases R-3, R-4). If the cellular secondary currents exist in an open-channel

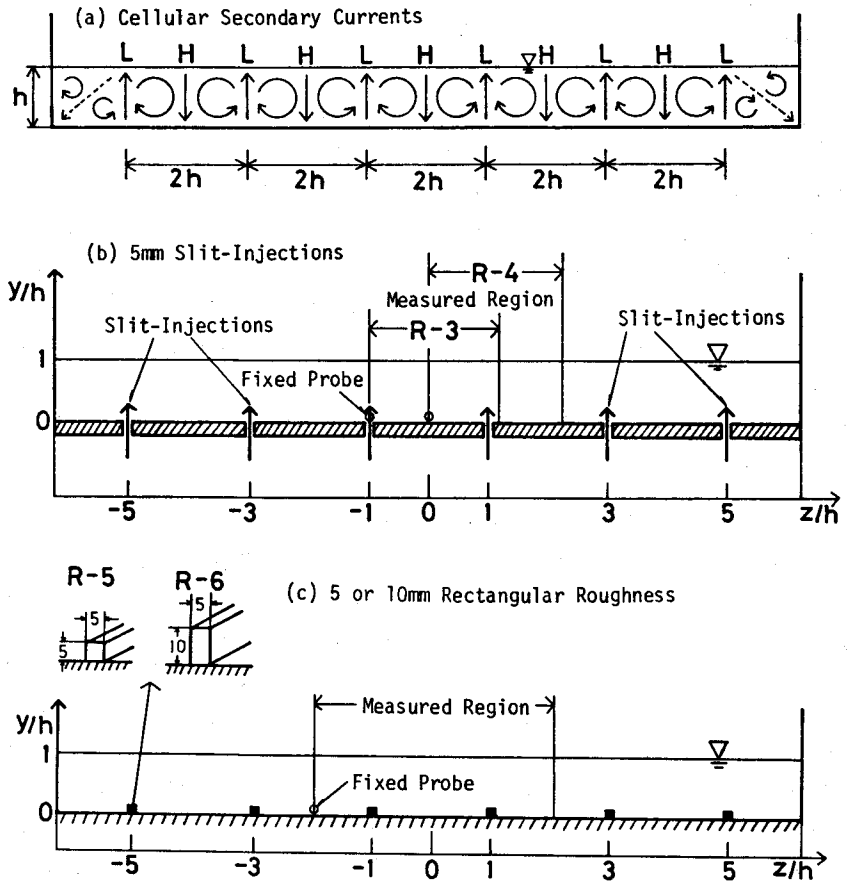

Fig. 2. Illustration of cellular secondary currents and the experimental set-up.

flow, they must have the same configuration as described in Fig. 2(a). In order to artificially create significant cellular secondary currents in the open channel, 5 mm-slit injection flows were given through the porous plate, at spanwise intervals of $2h$, as shown in Fig. 2(b). The apparatus of the uniform flow of injections through a porous plate of 1040 mm long, 490 mm wide and 15 mm thick, has been described in detail in our previous paper (1979).[25] On the basis of this experience, the test section was chosen at the position of 840 mm downstream from the upstream edge of the porous plate. The injection velocity v_0 was equal to about a half of the friction velocity U_*. In order to examine the effect of the injection on the bursting detection probe, the probe was set at the injection point for Case R-3, and at the intermediate point between the adjacent injections for Case R-4, respectively, although the hydraulic conditions were nearly equal in both cases. (*See Fig. 2*).

Flow with rectangular longitudinal roughness elements (Cases R-5 and R-6). Utami & Ueno (1977)[26] pointed out that stable cellular secondary currents appeared in open-channel flows when the rectangular roughness elements were aligned in the mean flow direction at spanwise intervals of $2h$, as described in Fig. 2(c). Similar effects will appear in the current lineations which are spanwise alternating ridges and broad hollows (Jackson 1976[15]). Hence, in the present study, the rectangular and polished brazen roughness elements with a 5×5 mm cross-section for Case R-5 and a 5×10 mm cross-section for Case R-6, respectively, were aligned parallel to the mean flow. (*See Fig. 2(c)*.) These longitudinal roughness elements with tapered upstream edge were 6000 mm long, and the position of the test section was chosen 5000 mm downstream from its tapered edge. The hydraulic conditions of Cases R-5 and R-6 were nearly the same as those of Cases R-3 and R-4.

3.2 Probe Measurements and Date Procedures

A V-type dual sensor (DISA 55A89) and an I-type single sensor (DISA 55A85) hot-films were used as the detection (fixed) probe and the sampling (movable) probe, respectively. As shown in Fig. 2, the position z_0 of the detection probe was fixed at the center of the channel, so that $z_0/h=0$ for Cases R-1 and R-2, $z_0/h=-1$ for Case R-3, $z_0/h=0$ for Case R-4 and $z_0/h=-2$ for Cases R-5 and R-6, respectively. The position z_1 of the sampling probe was systematically moved over distances longer than $2h$. It was set at about 90 different points in number for each run, in the y-z plane at $x_0\equiv x_1\equiv 0$. The vertical positions of the detection and sampling probes were set equally to each other, in which $y\equiv y_0\equiv y_1=$ 4, 7, 13, 24, 40 and 60 mm for R-1 and R-2, $y=4$, 10, 20 and 35 mm for R-3 and

R-4, and y=4, 7, 10, 20 and 35 mm for R-5 and R-6, in order to obtain the representative measured points in both the wall and outer regions. Of course, the probe was arranged so as to avoid any effect of the wake by another probe.

The output signals of the anemometers were recorded in analog form by using an FM tape recorder for about two minutes at each measured point. The effects of impurities and bubbles in the water on the hot-films were almost negligible in this duration, and thus a stable operation of the anemometers was obtained. The output signals were then reproduced for converting into digital form, with the sample size N=10,000 and the sampling frequency f=100 Hz, that is, the average evaluation time $T=N/f$=100 seconds. The sampling frequency f was chosen so that the spectral analysis could be performed at least to the extent of the inertial subrange (Nezu 1977,[2] also see Fig. 18).

The temperature difference between the water (T_w) and the hot-film sensor (T_s) was set at about 20°C through all tests. The maximum frequency response f_{max} of the hot-films is 30 kHz in the technical data of DISA, and it was confirmed by the spectral analysis (Nezu 1977[2]) that $f_{max}>1000$ Hz in ordinary hydraulic conditions, which was sufficiently high for the present study. The hot-film anemometers were calibrated by towing the probe over a fixed length of about 2 m in still water, by making use of a movable carriage driven by a variable motor before and after each run of measurements.

Consequently, the output voltage signals could be easily converted into the velocity signals through these calibration curves. Then, some statistical analyses described previously were carried out by a large digital computer, the FACOM M-200, at the Data Processing Center, Kyoto University. Most of the results were then plotted by an on-line X-Y plotter.

4. Experimental Results and Discussion

4.1 Mean Velocity and Turbulence Intensities

Fig. 3 shows the mean velocity distributions $U^+\equiv U/U_*$ measured by a detection probe at each test section of z_0, as described in **3.2.** The solid line is the well-known log-law distribution, which is given by the van Driest type for $y^+\leq 30$, where the Karman constant κ=0.4 and the van Driest damping constant A=27 are used.[1] The friction velocity U_* could be reasonably determined so that the experimental values of U, u', v' and $-\overline{uv}$ might coincide with the theoretical curves as accurately as possible. Obviously, the experimental values in Fig. 3 agree very well with the log-law profile. Fig. 4 shows the turbulence intensities u'/U_* and v'/U_*, measured by the detection probe. Their experimental values are in good agreement

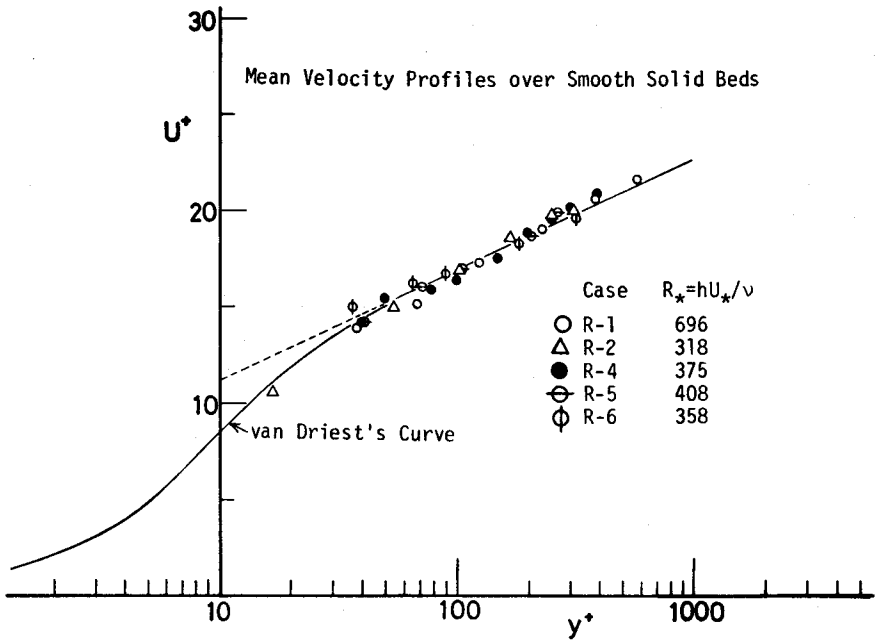

Fig. 3. Mean velocity distribution at the detection probe.

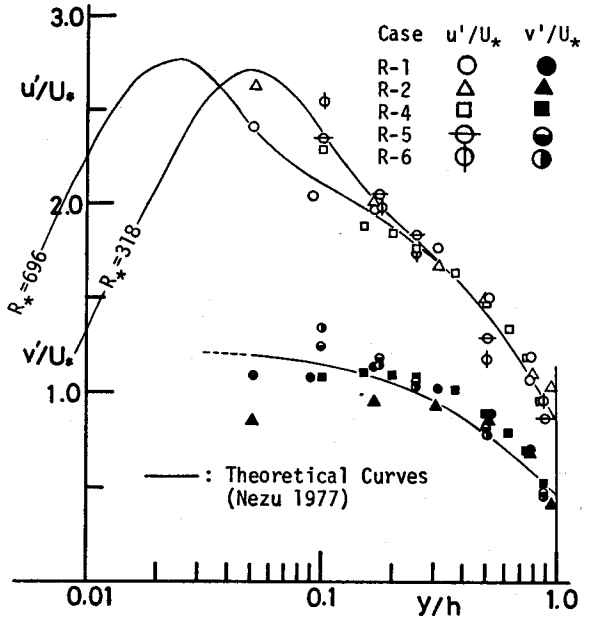

Fig. 4. Turbulence intensities at the detection probe.

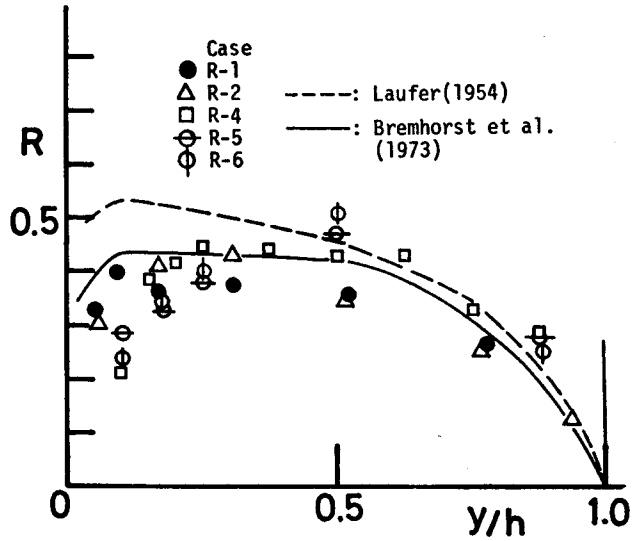

Fig. 5. Correlation coefficient of the Reynolds stress at the detection probe.

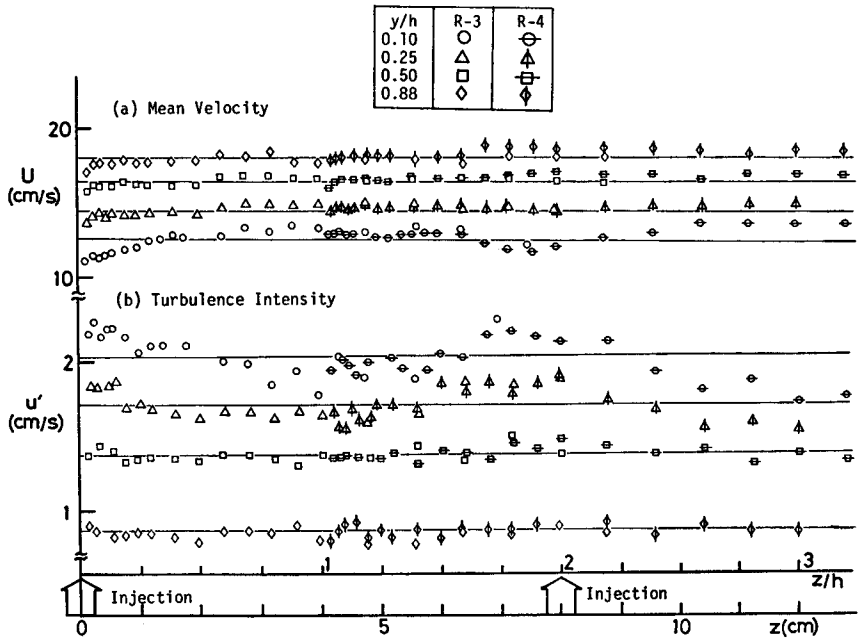

Fig. 6. Variations of mean velocity and turbulence intensity against the spanwise direction, z, when 5 mm slit-injections are given at spanwise intervals of $2h$.

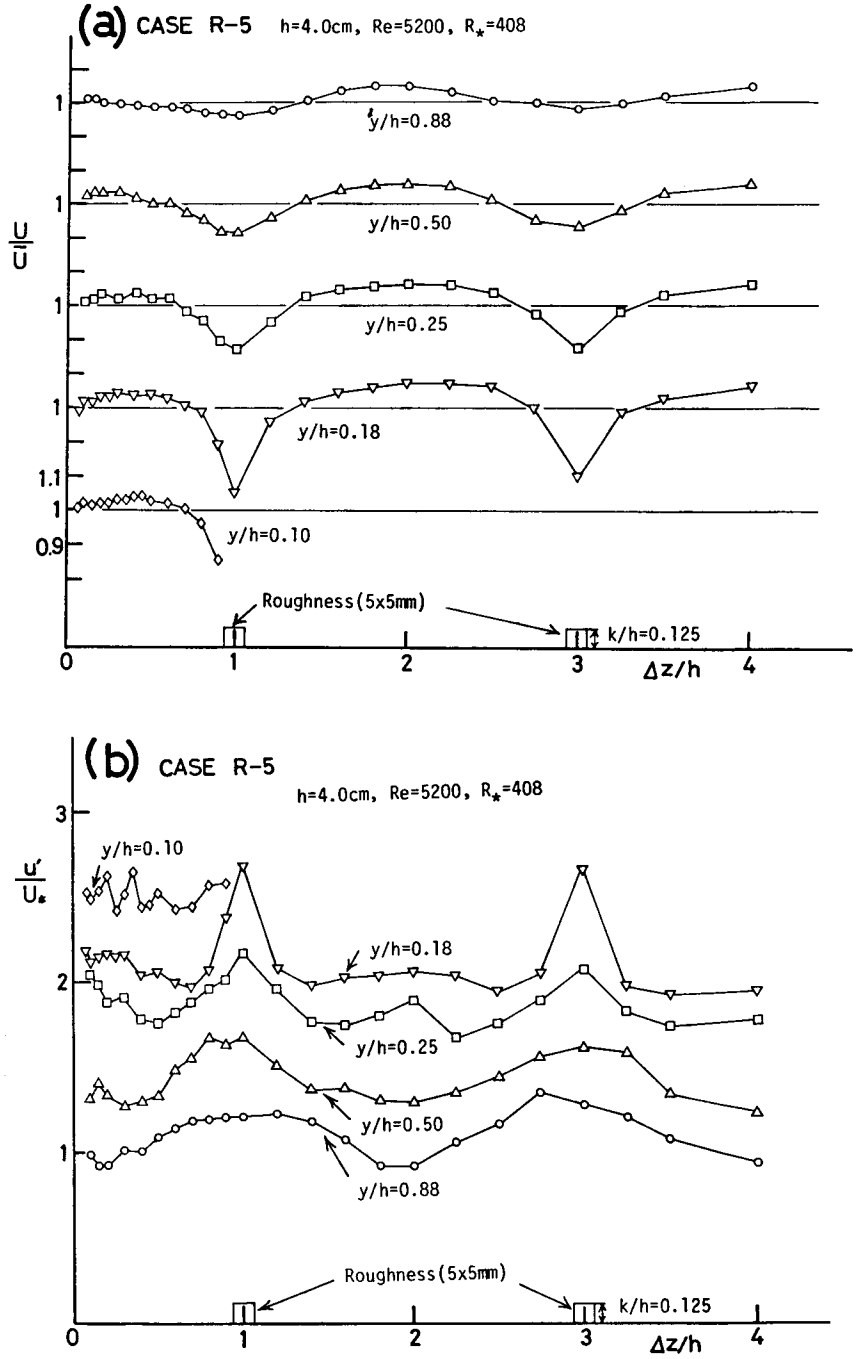

Fig. 7. Variations of mean velocity and turbulence intensity against the spanwise direction, $\Delta z/h$, when the longitudinal roughness elements are set at spanwise intervals of $2h$.

with the theoretical curves given by Nezu (1977).[2] Fig. 5 shows the correlation coefficient $R \equiv -\overline{uv}/u'v'$ of the Reynolds stress. The scatter of the present data is almost within that of the previous data.[27),28)] Further, the contribution rates of each bursting event to the Reynolds stress coincided well with the previous data of Nakagawa & Nezu (1977).[23)] From the above examination, it can be concluded that even in the flows with interval injections (Cases R-3 and R-4) and longitudinal roughness elements (R-5 and R-6), the turbulence characteristics of a two-dimensional and fully developed open-channel are satisfactorily established at the position of the detection probe. Therefore, the bursting phenomenon can be accurately detected by the present probe measurements.

Next, Fig. 6 shows the variation of the mean velocity $U(y,z)$ and the turbulence intensity $u'(y,z)$ obtained by the sampling probe measurements at the different elevations, when the 5 mm-slit injections were given spanwise at intervals of $2h$. Obviously, a region of the low mean velocity and high turbulence intensity appears at intervals of $2h$ in the vicinity of the wall. This feature is very consistent with that of a secondary current in Fig. 1 (e.g. Müller 1977[29)]). However, the above feature becomes more indiscernible as the water surface is approached, probably due to a strong diffusion of the injections. Consequently, a large-scale cellular secondary current across the whole flow depth was not created here in Cases R-3 and R-4.

In the same manner, Fig. 7 plots the spanwise variation of $U(z)$ and $u'(z)$ for Case R-5, where the long longitudinal roughness elements of $k=5$ mm high were set spanwise at intervals of $2h$. The measurement zone Δz was up to h at the elevation of $y/h=0.1$, which was under the top of the roughness elements, i.e. $k/h=0.125$. At the other elevations of y/h, Δz was up to $4h$. The spanwise average values of $U(z)$ and $u'(z)$ are denoted as $\bar{U}$ and $\bar{u}'$, respectively. The low mean velocity ($U<\bar{U}$) and high turbulence intensity ($u'>\bar{u}'$) appear near the position of $\Delta z/h=1$ and 3, while the high mean velocity ($U>\bar{U}$) and low turbulence intensity ($u'<\bar{u}'$) appear in the vicinity of $\Delta z/h=0$, 2 and 4. These cyclic variations of $U(z)$ and $u'(z)$, whose wave lengths are equal to $2h$, are seen clearly throughout the water depth. The same results were also obtained for Case R-6, where the roughness height was $k/h=0.25$. The r.m.s. values $\Delta U'$ and $\Delta u'$ of the mean velocity difference $\Delta U \equiv U-\bar{U}$ and the turbulence intensity difference $\Delta u \equiv u'-\bar{u}'$, respectively, in respect to the spanwise direction z, are shown in Fig. 8, together with the correlation coefficient $R_\Delta \equiv -\overline{\Delta U \Delta u}/\Delta U' \Delta u'$ between the two. By comparison between Figs. 3, 4 and Fig. 8, these values of $\Delta U'$ and $\Delta u'$ are less than 10 percent of $\bar{U}$ and $\bar{u}'$, respectively. However, it should be noticed that R_Δ has positive values against the whole variation of y/h. In particular, it shows a

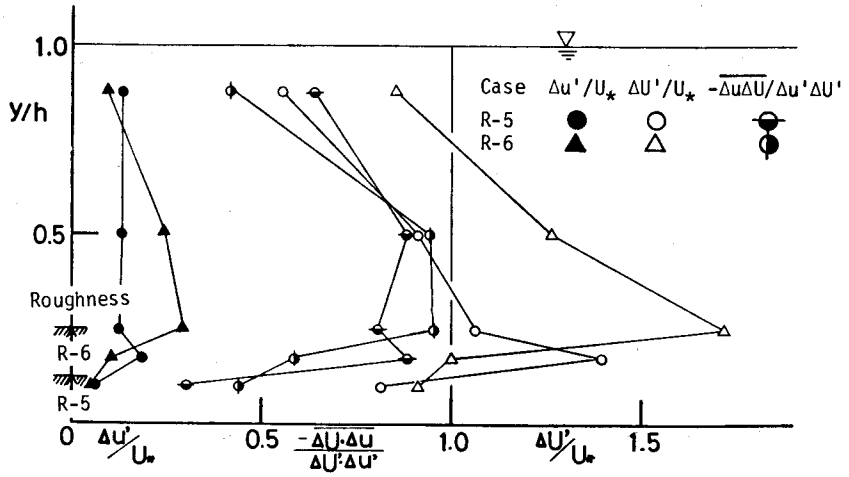

Fig. 8. Correlation coefficient between the mean velocity $U(z)$ and turbulence intensity $u'(z)$.

large positive correlation between ΔU and $-\Delta u$ at the middle of the flow depth, that is, $R_\Delta \simeq 0.9$ at $y/h \simeq 0.5$. The typical cellular secondary currents in Fig. 2 produce the largest ascending current, which probably corresponds to $\Delta u > 0$, in the zone of the low mean velocity ($\Delta U < 0$), and also the largest descending current, which probably corresponds to $\Delta u < 0$, in the zone of the high mean velocity ($\Delta U > 0$), at the middle position of the flow depth. Hence, the present experimental values of R_Δ may satisfactorily explain these features of the secondary currents (cf. Müller 1977[29]). In other words, the cellular secondary currents must have been created throughout the flow depth by setting the longitudinal roughness elements at spanwise intervals of $2h$.

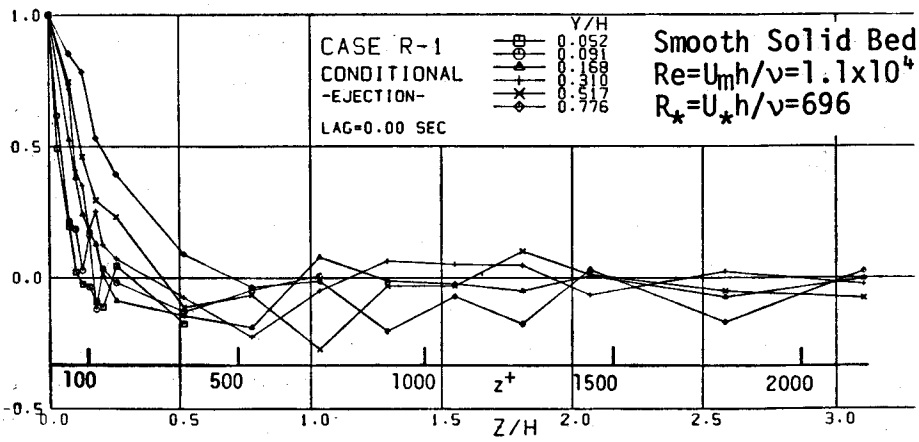

Fig. 9. Spanwise spatial structure of the ejection (Case R-1).

4.2 Spanwise Streaky Structure of Bursting Motions

It is well recognized by many visual observations[30] that the spanwise spatial structure in the wall region consists of high- and low-speed streaks, whose mean spacing $\bar{\lambda}$ is nearly equal to constant, i.e. $\bar{\lambda} \simeq 100\nu/U_*$. Our earlier visual study (1977)[31] of an open-channel flow had also found that, although there clearly existed a streaky structure of $\bar{\lambda}^+ \simeq 100$ in the wall region, it became gradually indistinct outside the wall region. Also, its spacing $\bar{\lambda}^+$ tended to increase with

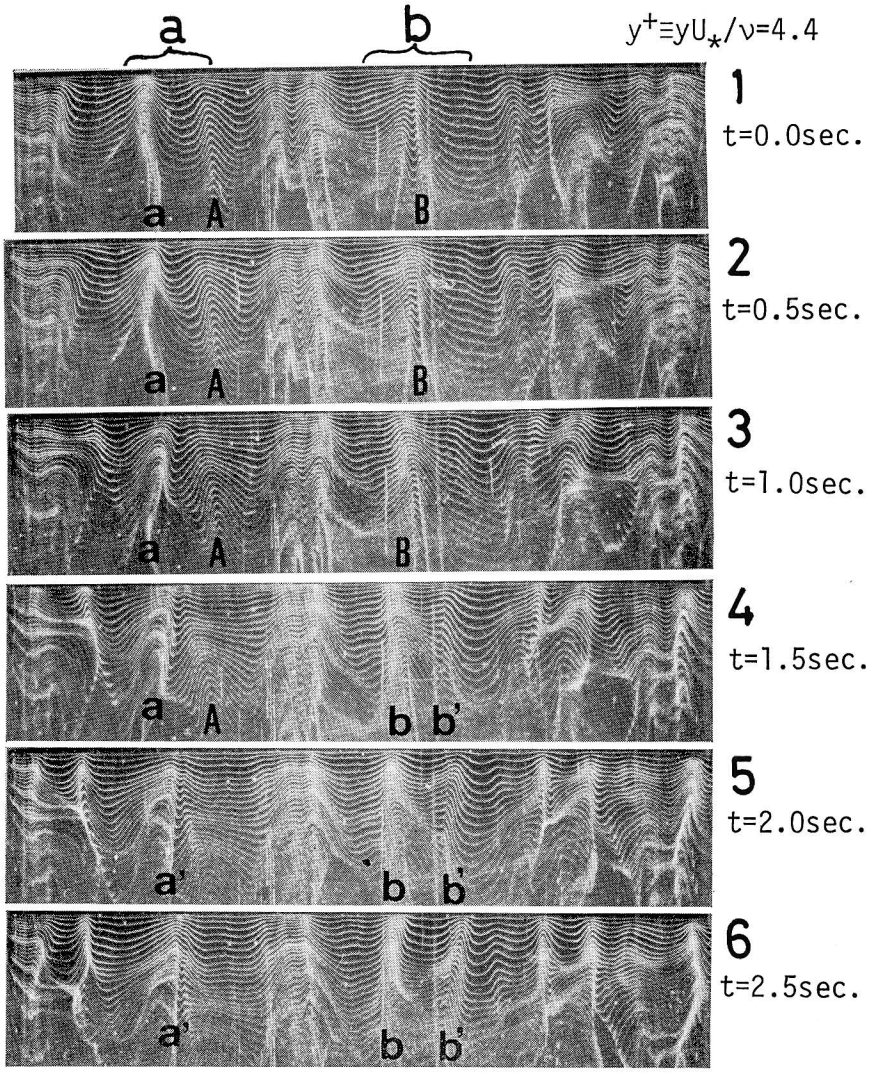

Photo 1. Streaky structure in the viscous sublayer ($y^+ = 4.4$) visualized by means of hydrogen-bubble tracer. The sequence of six motion film frames, separated in time by 0.5 sec, illustrate a coalescence (shown by a-A) and a division (shown by b-B) of the streaks.

y/h. In order to obtain a more quantitative evaluation, the spatial structures of $\langle u\rangle_e(y, z, \tau)$ and $\langle u\rangle_s(y, z, \tau)$ were analyzed by making use of the conditional average of Eqs. (3) and (4), where $\Delta x \equiv 0$, $y \equiv y_0 \equiv y_1$ and $z \equiv z_1 \equiv \Delta z$.

Fig. 9 shows an example of the conditionally averaged spanwise structure $\langle u\rangle(y, z, 0)$ obtained at $Re = 1.1 \times 10^4$ (Case R-1), in which $\langle u\rangle_e(y, z, 0)$ of the ejections is normalized by $\langle u\rangle_e(y, 0, 0)$. Similar results were also obtained for the sweeps. Evidently, the spanwise spatial scale increases with an increase of y/h. However, the existence of the stable cellular secondary current shown in Fig. 1 is not clear, because $\langle u\rangle(z)$ decays fairly rapidly up to $z/h = 2$. Surely, some periodicity of $\langle u\rangle(z)$ is recognized near the wall, and it perhaps corresponds to the high- and low-speed streaks observed visually. Its intensity, however, is not so large, as compared with the results of Gupta et al. (1971)[18] who analyzed the spatial structure in the viscous sublayer by the VITA-method of the ten-hot-wire-rake signals, and Nishioka et al. (1977)[32] who detected the bursting motions at $y^+ = 10$ by a three-hot-wire rake probe. (*See Figs. 11 and 12.*) This difference can be explained in the following manner. (1) If a multi-point-rake probe of more than two sensors is used as a detection probe, the detection criterion of the bursting motions will be

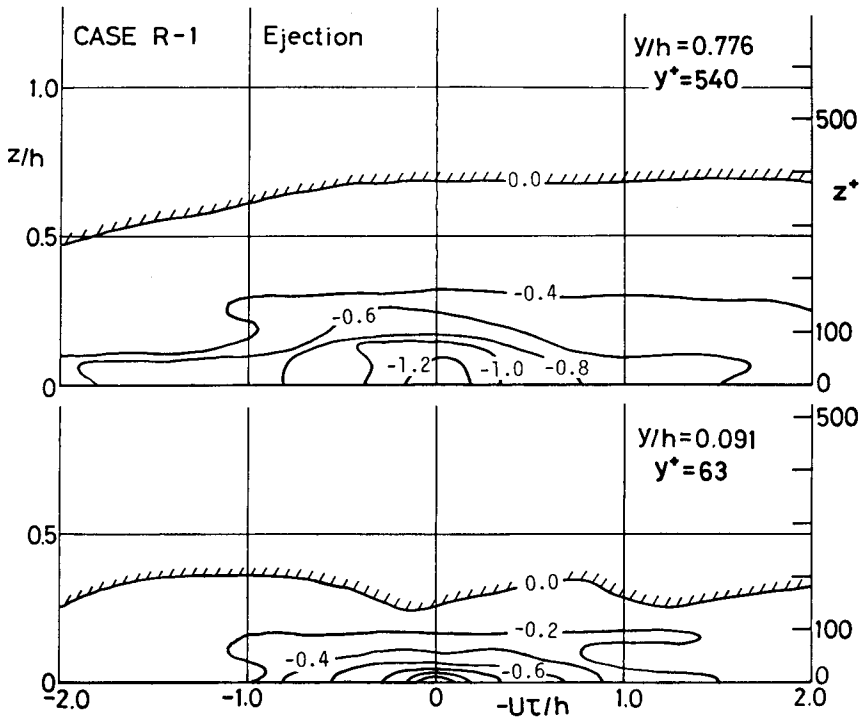

Fig. 10. Space-time iso-contours of $\langle u/u'\rangle$ in the ejection phase.

able to be set more precisely and reasonably. (2) In the viscous sublayer($y^+ \leq 10$), the coherent streaky structure appears, in itself, more clearly (Nakagawa & Nezu 1977,[31] also see Ploto 1). It is, however, difficult at present to use the multi-point-rake probe in water flow. Moreover, it has been found that the wall streaks became gradually intricate and indistinct farther from the wall ($y^+ \geq 10$). Hence, in order to examine the streaky structure in both the wall and outer regions, a new analytic method will be necessary such as will be proposed in the next section.

Next, Fig. 10 shows an example of a space-time structure of the ejections, in which the contour lines of $\langle u/u' \rangle (z, \tau)$ are described at intervals of 0.2. Similar figures were also obtained for the sweeps. Because the convection velocity of the ejection motions is nearly equal to about 0.8 times the mean velocity U (Nakagawa et al. 1980[17]), the value of $U \times (-\tau)$ cannot be precisely regarded as the convectin distance Δx, but only as a rough approximation of Δx. It should be noticed that the bursting structure enlarges as it goes farther from the wall, and that it indicates a longitudinally elliptic shape extended in the streamwise direction. This shape is similar to the structure of the conventional space-time correlations evaluated by a long-time average. Thus, it is recognized that the bursting motion is a kind of large-scale eddy structure, as the authors (1980)[17] pointed out with regard to the x-y plane structure.

4.3 Evaluation Method of Mean Streaky Spacing

Lee et al. (1974)[33] observed prints of the coherent streaky structure on the wall by making use of electrochemical techniques, and they reported that the instantaneous velocity pattern of the wall streaks was approximately expressed by a cyclic function such as $\cos(2\pi z/\lambda)$, where λ is the wave length of the spanwise wall streaks. That is,

$$u(z, t) = u(0, t) \cdot \cos(2\pi z/\lambda) \sim \lambda \cdot \cos(2\pi z/\lambda) \tag{5}$$

By ensemble averaging $u(z, t)$ in respect to its wave length λ, we can obtain

$$\frac{\langle u \rangle (z)}{\langle u \rangle (z=0)} = \frac{\int_0^\infty \lambda \cdot \cos(2\pi z/\lambda) \cdot P(\lambda) d\lambda}{\int_0^\infty \lambda \cdot P(\lambda) d\lambda} \tag{6}$$

where, $P(\lambda)$ is the probability of the occurrence of λ. Eq. (6) is equivalent to $\langle u \rangle (z)$ of Eq. (1), whose average is weighted by λ itself. Our visual observation (1977)[31] had found that $P(\lambda)$ was expressed well by the log-normal distribution:

$$P(\lambda) = \frac{\log e}{(2\pi)^{1/2} \sigma_0 \lambda} \cdot \exp\left\{ -\frac{1}{2} \left(\frac{1}{\sigma_0} \log \frac{\lambda}{\lambda_0} \right)^2 \right\} \tag{7}$$

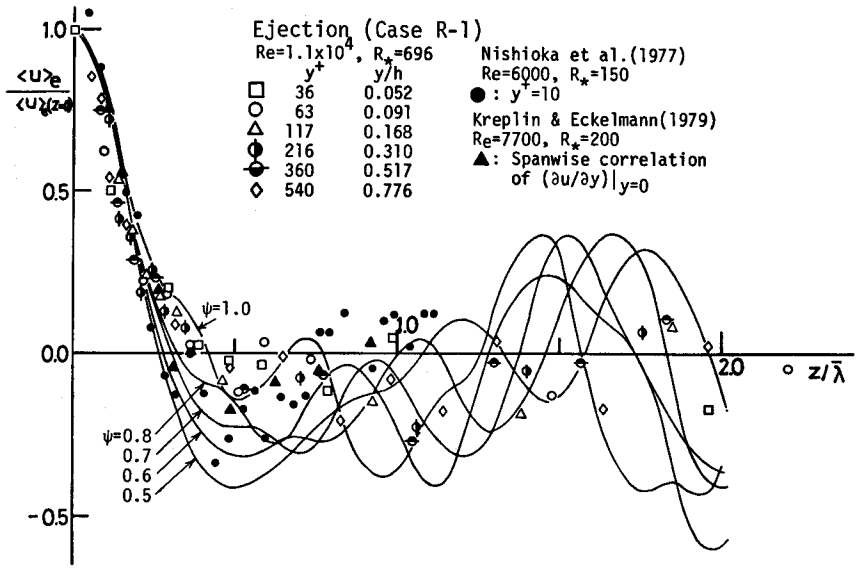

Fig. 11. Spanwise spatial structure of the elections normalized by the mean streaky spacing $\bar{\lambda}_e$.

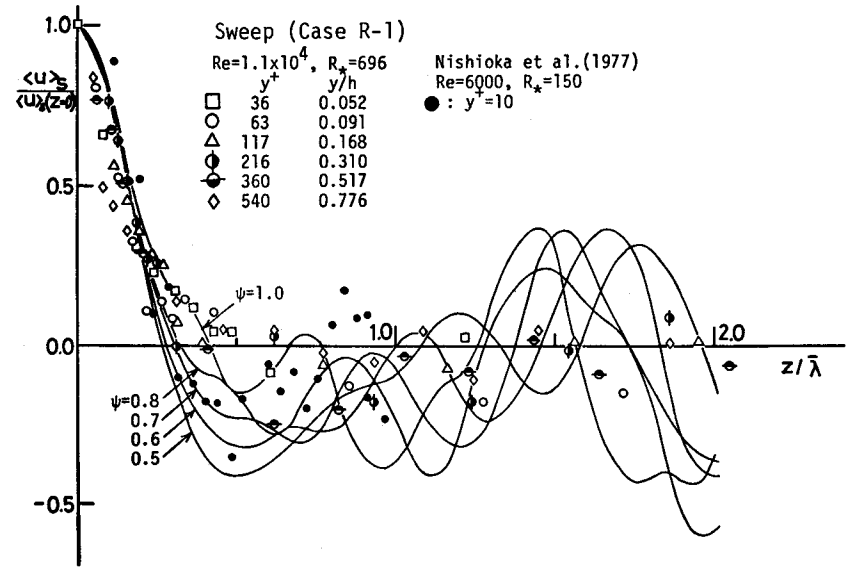

Fig. 12. Spanwise spatial structure of the sweeps normalized by the mean streaky spacing $\bar{\lambda}_s$.

where, $\sigma_0 \equiv (\log e)\ (\ln(1+\psi^2))^{1/2}$, $\lambda_0 \equiv (1+\psi^2)^{-1/2} \cdot \bar{\lambda}$ and $e=2.71828$. The calculated curves of Eq. (6) are shown versus $z/\bar{\lambda}$ in Figs. 11 and 12, as a parameter of $\psi \equiv \sigma/\bar{\lambda}$, where λ is the mean value of λ, and σ is the standard deviation of λ. Even the curve of Eq. (6) with $\psi=0.5$† evaluated from our visual data[31] does not show any

† The value of the coefficient ψ of the variation of the bursting period is nearly equal to 0.5–1.5 (Nakagawa & Nezu 1978[16]).

ticeable periodicity. This means that the high- and low-speed streaks are fairly smoothed even by means of the conditional average of the two probe signals.

The effect of ψ on Eq. (6), however, is fairly small up to the first zero-crossing point z_c. Then, by using $\psi=0.7$†, the following equation can be obtained from Eq. (6).

$$\int_0^{z_c} \frac{\langle u\rangle(z)}{\langle u\rangle(z=0)}\,dz = 0.16\bar{\lambda} \tag{8}$$

The mean spacing $\bar{\lambda}$, therefore, can be determined tentatively to satisfy Eq. (8) with the experimental values in Fig. 9. The experimental values of $\langle u\rangle$ are plotted in Fig. 11, versus $z/\bar{\lambda}$, i.e. the spanwise separation distance normalized by the mean spacing $\bar{\lambda}$ evaluated from Eq. (8). Fig. 11 also shows the data obtained in an air pipe by Nishioka et al. (1977).[32] It also shows the recent data of Kreplin & Eckelmann (1979),[34] who measured the spanwise correlations of the velocity gradient at the wall by flush-sensor hot-films in an oil channel. A good agreement between the experimental and calculated values is recognized up to $z/\bar{\lambda}\simeq 0.5$, which corresponds to the spacing between the neighbouring high- and low-speed streaks. Therefore, the present evaluation method of $\bar{\lambda}$, which corresponds to a kind of integral scale (*See Eq. (8).*), seems to be reasonable. Also, these spatial features are true of the sweeps, as shown in Fig. 12.

4.4 Spanwise Streaky Structure in Uniform Flow over a Smooth Bed

Fig. 13 shows the mean streaky spacings $\bar{\lambda}^+\equiv\bar{\lambda}U_*/\nu$ versus y^+ for the ejections and sweeps in a uniform flow over a smooth bed (Cases R-1 and R-2), which were systematically evaluated from Eq. (8). For a comparison, in Fig. 13 are replotted the typical visual data of Nakagawa & Nezu (1977)[31] who used hydrogen-bubble techniques, and the previous anemometry data of Morrison et al. (1971),[35] Gupta et al. (1971)[18] and Nishioka et al. (1977).[32] Although there is some scattering among these experimental results, a good agreement between the previous and present data is recognized. This means, therefore, that the present evaluation method of the mean streaky spacing $\bar{\lambda}$ is quite reasonable.

$\bar{\lambda}^+$ is nearly constant, i.e. $\bar{\lambda}^+\simeq 100$, in the buffer layer ($y^+\leq 30$). It is surprising that Morrison et al. (1971)[35] could obtain the streaky spacing $\bar{\lambda}^+=135$ in the viscous sublayer ($y^+\leq 5$) by the long-time averaging spectral method, in contrast to the remarks of Gupta et al.[18]. Lee et al. (1974)[33] and Kreplin & Eckelmann (1979)[34] could also obtain the streaky spacing $\bar{\lambda}^+\simeq 100$ of the velocity gradient at the wall by the long-time averaging correlation method. These results indicate that the streaky structure of the viscous sublayer can be detected even by the conventional long-time averaging methods. In other words, this suggests that

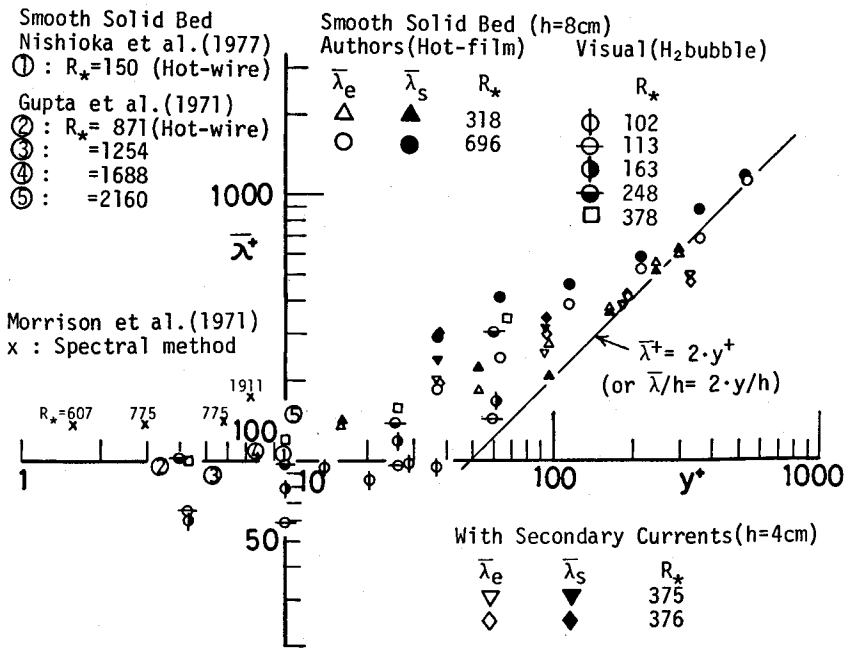

Fig. 13. Variation of the mean spacing $\bar{\lambda}^+$ between the high- and low-speed streaks, as a function of y^+.

the viscous sublayer may be regarded as a stable 'footprint' of the bursting motions.

Next, $\bar{\lambda}^+$ increases gradually in the region of $y^+ \geq 30$, and it is approximated by a relation of $\bar{\lambda}^+ = 2y^+$ in the outer region. This suggests that there may exist an interaction or pairing (coalescence) between the high- and low-speed streaks, and that its spacing on the water surface becomes nearly equal to $2h$, as shown in Fig. 1. As seen in the successive motion pictures of Photo 1, the wall streaks coalesce (*part*(*a*)) and break up (*part*(*b*)) by themselves repeatedly in space and time, and consequently their mean spacing $\bar{\lambda}^+$ is kept constant. The coalescence or pairing mechanism is recognized in common in coherent turbulent structures such as mixing layer, boundary layer, jets and wakes (e.g. Laufer 1975[6]). On the other hand, the break-up mechanism is caused by an inrush motion of accelerated fluids, i.e. sweeps, in the Offen-Kline model (1975).[10] Consequently, the coalescence of the streaky structure seems to be predominant over its break-up in the region of $y^+ \geq 30$, because the inrush motion becomes weaker farther from the wall (Grass 1971[14] and Nakagawa & Nezu 1977[23]). This can reasonably explain the above most important feature of the mean streaky spacing outside the buffer layer.

4.5 Spanwise Streaky Structure in Open-channel Flows with Cellular Secondary Currents

As an example, we consider Case R-5, where the essential features of the secondary currents appear throughout the flow depth, as mentioned before. The spanwise structure $\langle u\rangle_e(z)/\langle u\rangle_e(z=0)$ of ejections obtained by the measurements is shown in Fig. 14. As compared with Fig. 9 of Case R-1 where the secondary currents did not appear, a remarkable difference between the two cannot be recognized. This was also true of the other cases.

By the same evaluation method of Eq. (8) as in Cases R-1 and R-2, the mean spanwise streaky spacings $\bar{\lambda}_e$ and $\bar{\lambda}_s$ of the ejections and sweeps, respectively, were obtained for open-channel flows with cellular secondary currents. Figs. 15 and 16 are an inner variable description ($\bar{\lambda}^+$ *vs.* y^+) and an outer variable one ($\bar{\lambda}/h$ *vs.* y/h), respectively, of all the data in the present experiments. The most striking results is that the spanwise spacings $\bar{\lambda}_e$ and $\bar{\lambda}_s$ near the wall in Cases R-3, R-4, R-5 and R-6, coincide well with those obtained over the uniform solid bed of Cases R-1 and R-2, no matter how definite the feature of the secondary currents appears in this region, as shown in Figs. 6 and 7. $\bar{\lambda}/h$ increases monotonously with an increase of y/h, and tends to approach a relation of $\bar{\lambda}/h=2y/h$. However, near the water surface, i.e. $y/h=0.88$, the values of $\bar{\lambda}/h$ for R-3$\sim$R-6 are somewhat less than those for R-1 and R-2. Considering that the definite feature of the secondary currents could not be detected near the water surface in the cases of R-3 and R-4, as mentioned earlier in Fig. 6, this difference between the two is probably caused not by the secondary currents, but by other effects such as small water waves. (The flow depth h was nearly equal to 8 cm for R-1 and R-2, while it was nearly

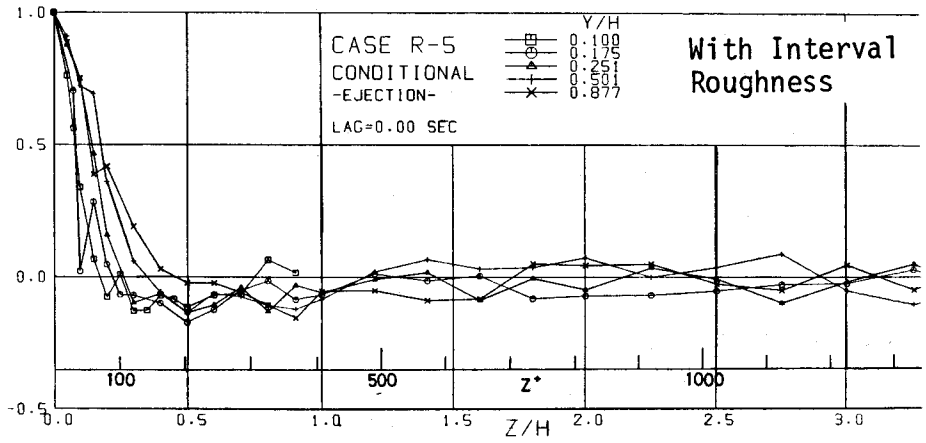

Fig. 14. Spanwise spatial structure of the ejections (Case R-5).

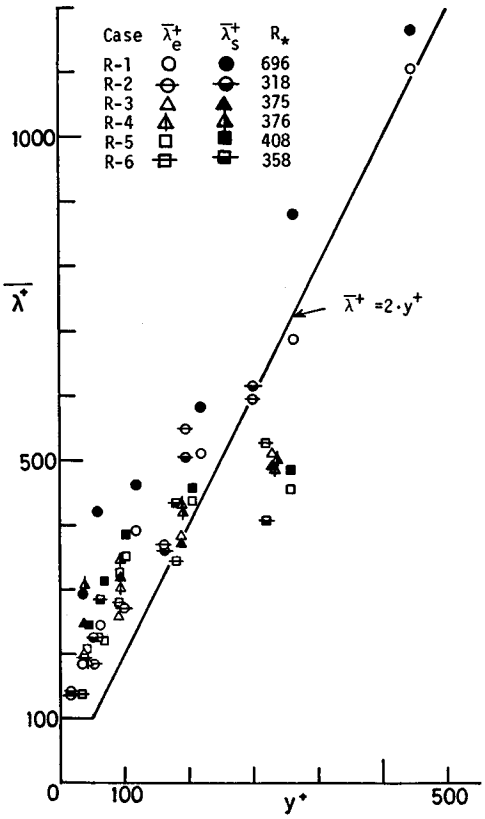

Fig. 15. $\overline{\lambda}^+$ *vs.* y^+ (inner variable expression).

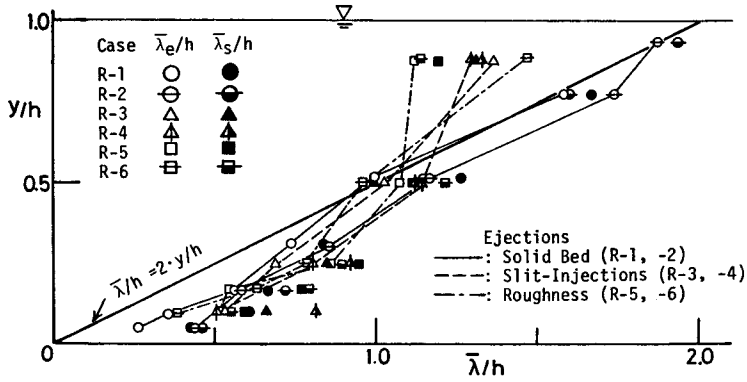

Fig. 16. $\overline{\lambda}/h$ *vs.* y/h (outer variable expression).

equal to 4 cm for R-3～R-6.)

Fig. 17 shows the ratio, $\overline{\lambda}_s/\overline{\lambda}_e$, of the sweep scale to ejection scale, against y/h. Although some scattering is seen among the data, a systematic variation affected by the secondary currents cannot be recognized. That is to say, irrespective

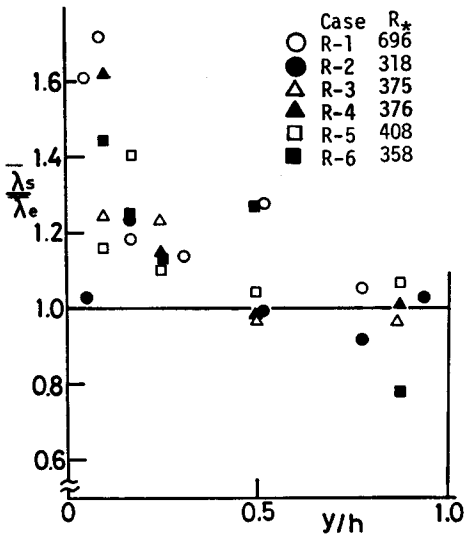

Fig. 17. Ratio $\overline{\lambda}_s/\overline{\lambda}_e$ of the sweep scale to ejection scale.

of the existence of secondary currents, the spanwise scale of the sweeps is larger than that of the ejections, i.e. $\overline{\lambda}_s > \overline{\lambda}_e$, near the wall where these bursting motions occur most violently. This feature has been also found by many visual observations[13] and conditional probe measurements (e.g. Nakagawa et al. 1980[17]). On the other hand, $\overline{\lambda}_s$ becomes equal to $\overline{\lambda}_e$ as the water surface is approached. This suggests strongly that the bursting motions tend to have an isotropic property near the water surface, which has been also suggested by Nakagawa & Nezu (1977)[23] in the examination of the contribution rates of bursting events to the turbulence production.

The above experimental results indicate that the high- and low-speed streaks of the bursting motions may not have a direct interrelation with the cellular secondary currents which scale with the outer variables. That is to say, the former cannot be identified with the latter.

4.6 Interrelation between the Bursting and Cellular Secondary Currents in the Productive Subrange of Spectrum

As mentioned in the Introduction, the large-scale eddies, such as kolk-boils and cellular secondary currents, in the outer region have been termed 'macroturbulence', in consideration of their kinematic behaviours. On the other hand, because the bursting phenomenon can be regarded as the mechanism by which the turbulent energy is produced from the mean flow, its phenomenon belongs almost to the productive subrange in the energy spectral space, which is controlled by a large-scale eddy represented by the integral scale L_x. It is, therefore,

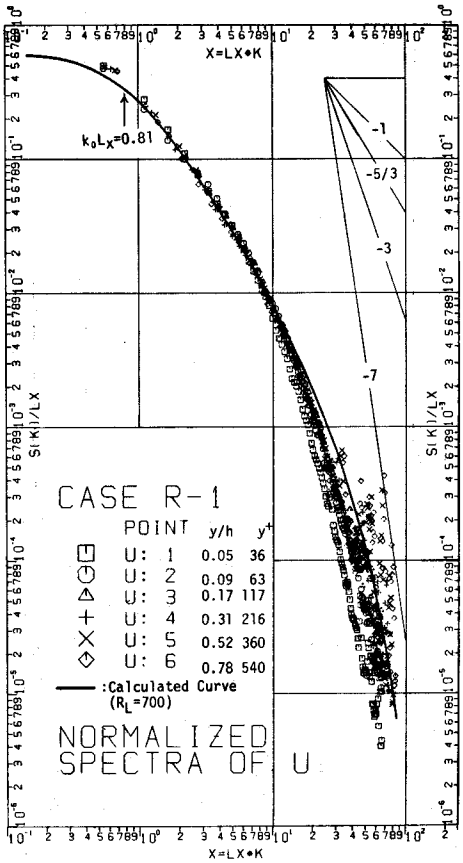

Fig. 18. Spectral distribution $S(k)$ at the detection probe (Case R-1).

considered that the macroturbulence and bursting motion both belong to a wave number range lower than the inertial subrange in which the well-known $-5/3$ power law is satisfied. In this section, we particularly examine an interrelation between the bursting and secondary currents in the productive subrange.

Fig. 18 is a typical example of the spectral distribution $S(k)$ in Case R-1, where k is the wave number. These spectral analyses were carried out by making use of the F.F.T. method with the sampling data size of 32,768. Also, similar results were obtained in the other experimental cases. Nezu (1977)[2] proposed a theoretical spectral distribution, as follows. In a range lower than the inertial subrange, the following Karman's interpolated formula is adopted:

$$S(k) = (2/\pi)\{1+(k/k_0)^2\}^{-5/6} \qquad (9)$$

In a range higher than the inertial subrange, Heisenberg's interpolated formula is adopted. Then, if the Reynolds number $R_L \equiv u'L_x/\nu$ is given, both formulae can

be further interpolated so that the dissipation spectrum may satisfy the relation of isotropic turbulence. Although the value of R_L gets smaller as the wall is approached, it becomes nearly constant in the outer region, i.e. $R_L=(u'/U_*)\,(L_x/h)R_* \simeq R_*$. The solid curve shown in Fig. 18 is a calculated one by the above theory, by using $R_L=700$, which is the average value in the outer region. The deviation between the experimental and calculated values in the viscous subrange is probably due to the limitations of hot-film measurements. However, a very good agreement between the two is recognized in a range lower than the inertial subrange, and thereby confirms the validity of Eq. (9). Then, the lower limit k_0 of the inertial subrange can be given by Eq. (9), and

$$k \leq k_0 \quad (\text{i.e.}\, f \leq f_0 \text{ in terms of frequency}) \tag{10}$$

corresponds to the productive subrange. In the present study, the value of k_0 was nearly equal to $0.8L_x^{-1}$ in all the experimental cases.

Incidentally, the present weighted average technique cannot detect each bursting motion separately, as mentioned in Chapter **2**. Therefore, by making use of the pattern-recognized techniques of Wallace et al. (1977)[22] where arbitrary parameters can be determined comparatively easily, the bursting period T_B was analyzed. Fig. 19 is a typical illustration of the pattern-recognized struc-

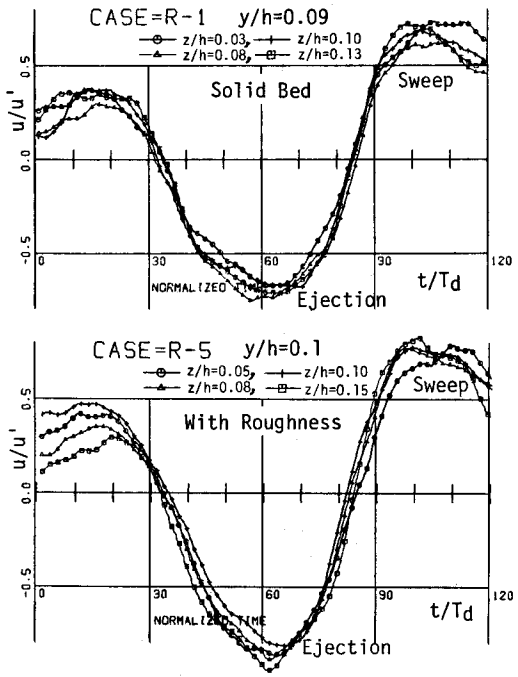

Fig. 19. Some examples of pattern-recognized structure of u/u'.

ture of u/u' which was measured by the single sampling probe at $y/h \simeq 0.1$ in Cases R-1 and R-5. Similar patterns were also obtained at the other measured points and in the other cases. It should be noted that the effects of the secondary currents on the bursting patterns of Case R-5 can hardly be seen, as compared with those of R-1.

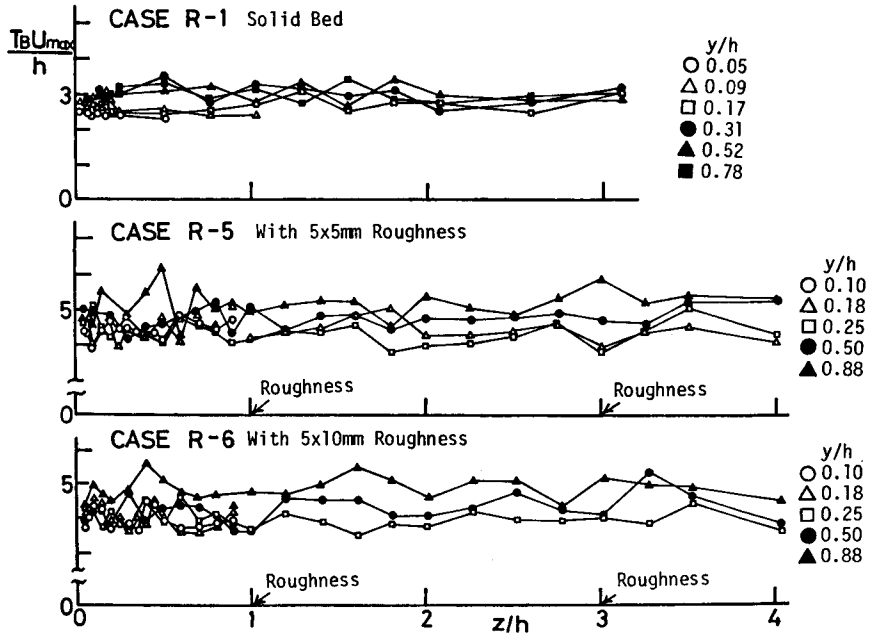

Fig. 20. Variation of mean bursting period $\bar{T}_B$ against z/h.

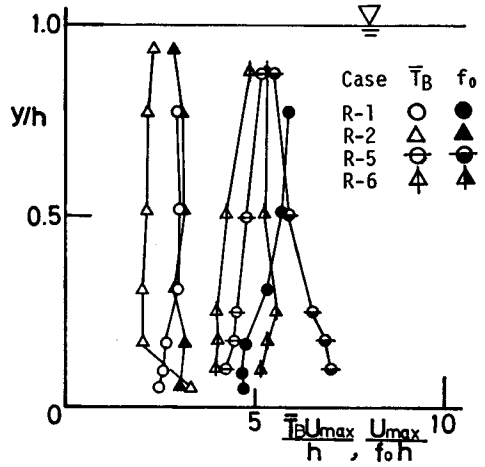

Fig. 21. Mean bursting period $\bar{\bar{T}}_B$ averaged in regard to z and the upper-limit frequency f_0 of the productive subrange.

Fig. 20 shows the mean bursting period $\bar{T}_B$ which was evaluated by the pattern recognized techniques, against the spanwise direction z/h. There is some scattering among these data, since the total number of occurrences of each bursting is only about 120 during the measurement time, i.e. 100 seconds. However, the spanwise distribution of $\bar{T}_B$ is nearly uniform in all cases. In other words, the effects of the secondary currents on the bursting period cannot be recognized. This result coincides with the notable result of Blackwelder & Woo (1974)[36] that the mean bursting period in the wall region during the disturbance is independent of the

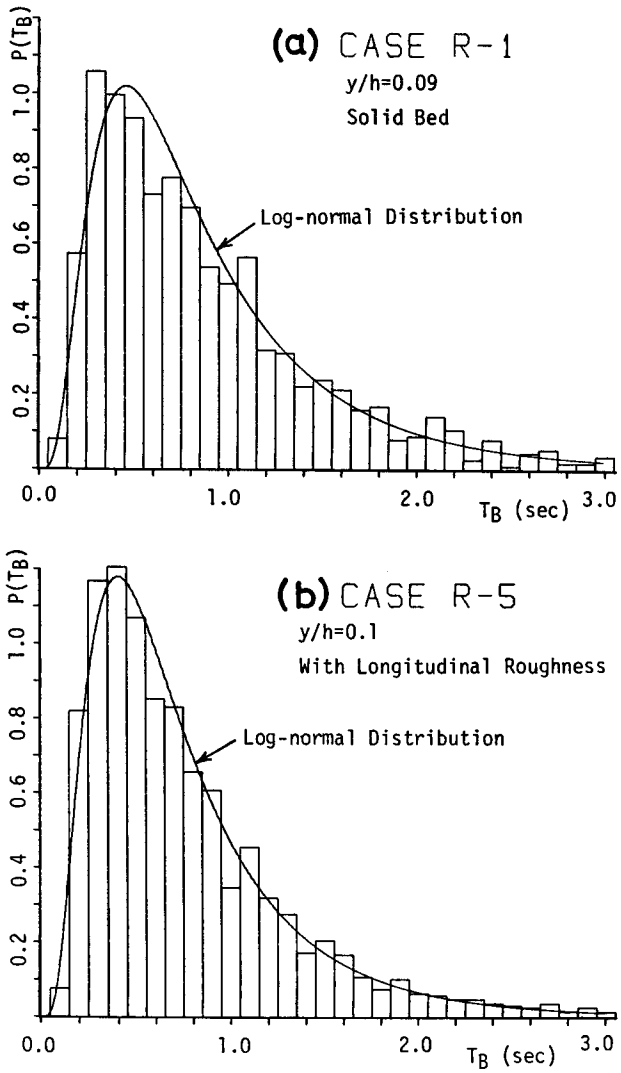

Fig. 22. Probability distribution $P(T_B)$ of the bursting period T_B.

pressure perturbation frequency given artificially in the outer region.

Fig. 21 shows the average value $\overline{\overline{T}}_B$ of the mean bursting period as regards the spanwise direction, and the upper limit frequency f_0 of the productive subrange, i.e. Eq. (10). Although $\overline{\overline{T}}_B$ is somewhat smaller than $1/f_0$, both of them are nearly constant against y/h. That is,

$$\overline{\overline{T}}_B U_{max}/h = (3-5) \tag{11}$$

Eq. (11) is also consistent with many previous data obtained in boundary layer[7], pipe[24] and open-channel flows.[16]

Fig. 22 is a typical example of the probability distribution $P(T_B)$ of the bursting period T_B for Cases R-1 and R-5, which corresponds to the pattern-recognized structure of Fig. 19. The solid curve is the log-normal distribution which has been given by the authors (1978)[16]. Evidently, the experimental values indicated by the rod diagram in Fig. 22 agree well with the log-normal distribution, independent of the cellular secondary currents created artificially.

From the above examinations, it is expected that, if the higher frequency components of $f > f_0$ are filtered out of the raw velocity signals, an interrelation between the bursting and secondary currents will be revealed more clearly. The low-pass filter adopted here was a linear digital filter technique. The raw signals $u(t)$ were converted into Fourier components by the F.F.T. method. Next, only after the Fourier components of $f > f_0$ were reduced to zero, they were converted into the filtered signals $u_f(t)$ by the inverse F.F.T. method. In the same manner as the raw signals $u(t)$, the conditional average $\langle u_f \rangle(z)$ of the filtered signals $u_f(t)$ was obtained from Eq. (1). Then, the mean spanwise streaky spacings $\overline{\lambda}_{ef}$ and $\overline{\lambda}_{sf}$ of the ejections and sweeps, respectively, were evaluated by using Eq. (8). These are shown in Fig. 23. A similar figure was also obtained for

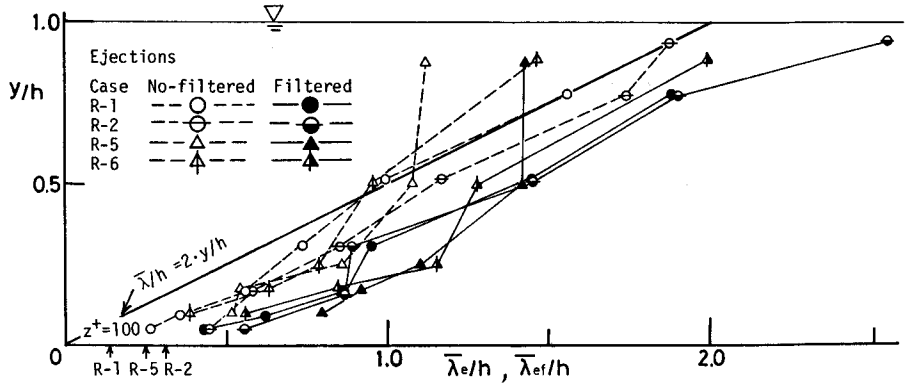

Fig. 23. Mean streaky spacing $\overline{\lambda}_{ef}$ of ejections in the filtered signals.

the sweeps. $\bar{\lambda}_{ef}$ indicates a uniformly increasing deviation from $\bar{\lambda}_e$, irrespective of y/h and the experimental cases. Above all, an outstanding feature is that the values of $\bar{\lambda}_f$ in the flow with the secondary currents (R-5 and R-6) coincide well with those in the uniform flow (R-1 and R-2). Consequently, the effects of the secondary currents on the bursting streaks cannot be recognized again.

At present, although there is no measurement data about the velocity of the ascending and descending currents of the cellular secondary currents, their velocity seems to be at most in the order of the vertical turbulence intensity v' (Jackson 1976[15]). Assuming that the cellular secondary current in Fig. 2 is represented as a circular motion with the diameter h and the rotating frequency f_s, we can obtain

$$U_{max}/(f_s h) \geq \pi (U_{max}/v') \tag{12}$$

Since $U_{max}/v' \geq 20$ from Figs. 3 and 4, Eq. (12) yields to $U_{max}/(f_s h) \geq 60$, which is much larger by one order than the bursting period $\overline{\overline{T}}_B$ of Eq. (11). This suggests strongly that the bursting and cellular secondary currents are phenomena different from each other.

5. Concluding Remarks

We summarize here the interrelation between the bursting phenomenon in the wall region and the macroturbulence in the outer region, on the basis of much fragmentary information obtained from the previous and present studies.

(1) *Evidences which suggest the existence of interrelation between the two phenomena*

(a) The mean period of occurrence of boils is coincident with the mean bursting period, i.e. Eq. (11). The probability distributions of their occurrences are both log-normal ones (Jackson 1976,[15] Nakagawa & Nezu 1978,[16] Fukuoka & Fukushima 1980[37] and the present study).

(b) The mean spanwise streaky spacing $\bar{\lambda}$ gradually increases in a vertical direction from $\bar{\lambda} \simeq 100\nu/U_*$ to $2h$ on the water surface (the present study).

(c) The transverse vortex in the outer region seems to trigger an occurrence of a new bursting motion in the wall region (Offen & Kline 1975,[10] Praturi & Brodkey 1978,[13] Nakagawa et al. 1980[17]).

(d) The bursting process is explained well by a horseshoe vortex model (Offen & Kline 1975,[10] Praturi & Brodkey 1978,[13] Nakagawa et al. 1978[16] & 1980[17]). The macroturbulence of kolk-boils is also explained by a horseshoe vortex model (Utami & Ueno 1977,[26] Fukuoka & Fukushima 1980[37]).

(2) *Evidences which deny the direct interrelation between the two phenomena*

(e) When the Reynolds number is sufficiently large, the thickness of the wall

region becomes very small, and thus the scales of the bursting and macroturbulence are very different from each other.

(f) The bursting motions occur randomly in space and time, while the boils and secondary currents occur at nearly fixed positions which are controlled by the flow depth (Kinoshita 1967,[4] Jackson 1976[15]).

(g) The effects of the cellular secondary currents on the bursting wall streaks cannot be recognized (the present study).

(h) The bursting phenomenon produces the turbulent energy from the mean flow, while the macroturbulence does not necessarily produce the turbulence and Reynolds stress.

Among the above items, (h) will be the most important hydrodynamic feature to make clear whether or not any interrelation exists between the two phenomena. The most essential mechanism of turbulent open-channel flow is the production of turbulent energy from its mean flow. Its energy is transferred into smaller eddies through the cascade process, and finally dissipates into heat by the viscosity. Thus, the bursting phenomenon is the most essential one in the wall turbulence. In other words, the flow over the wall without the bursting phenomenon is no longer turbulent. On the other hand, the turbulent flows in which the macroturbulence cannot be detected must exist in the nature. Actually, the macroturbulence cannot be usually observed in the laboratory straight smooth flumes, such as used in the present study. That is to say, the macroturbulence is not directly caused by the bursting motions, but it is probably caused by other factors such as various bedforms. For example, the large-scale eddies due to flow separation are produced on the crest of the sand wave bed.

However, we cannot conclude that the bursting and macroturbulence are quite independent phenomena, because some kinematic analogy of the items (1) exists between the two. In this discussion, we should recall the hypothesis of the double-structure of turbulence, which has been proposed by Falco (1977)[11] and Nezu (1977),[2] that the wall turbulence consists of both a bursting motion controlled by the inner variables and a macroturbulence controlled by the outer variables. According to this hypothesis, the former is the active component that contributes to the production of turbulence and the Reynolds stress, and indicates the universal characteristics. The latter is the inactive component that has a much lower frequency relating to the flow history from the upstream. This conception of active-inactive components is consistent with that which had been already proposed by Bradshaw (1967).[38]

The bursting motions occurring in the wall region will be convected outward from the wall and downstream (*See Fig. 1*) as if they were riding on the macrotur-

bulence. They will then decay and at last disappear in the outer region. Because the composite vortex of the macroturbulence and bursting motions, that is, a kind of transverse vortex, probably occasions a new bursting motion, its mean bursting period T_B becomes nearly constant throughout the flow depth as shown in Fig. 21. Both the bursting and macroturbulence must coexist self-consistently even when the Reynolds number becomes sufficiently large. Therefore, more detailed investigations will be needed to determine whether or not the macroturbulences of kolk-boils and cellular secondary currents in an actual river correspond to the inactive component. Then, the above hypothesis of a double-structure of turbulence can well explain the coherent structures in an open-channel flow.

References

1) Hinze, J.O.: *Turbulence* (2nd ed.), McGraw-Hill, pp. 586–770 (1975).
2) Nezu, I.: *Turbulent Structure in Open-channel Flows*, Ph. D. thesis, Kyoto University (1977).
3) Matthes, G.H.: Macroturbulence in natural stream flow, Trans. of Amer. Geoph. Union, vol. 28, pp. 255–265 (1947).
4) Kinoshita, R.: An analysis of the movement of flood waters by aerial photography, concerning characteristics of turbulence and surface flow, Photographic Surveying, vol. 6, pp. 1–17 (1967) (*in Japanese*).
5) Coleman, J.M.: Brahmaputra river; Channel processes and sedimentation, Sediment. Geol., vol. 3, pp. 129–239 (1969).
6) Laufer, J.: New trends in experimental turbulence research, Ann. Rev. Fluid Mech., vol. 7, pp. 307–326 (1975).
7) Willmarth, W.W.: Structure of turbulence in boundary layers, Adv. Appl. Mech., vol. 15, pp. 159–254 (1975).
8) Laufer, J. and Narayanan, M.A.B.: Mean period of the turbulent production mechanism in a boundary layer, Phys. of Fluids, vol. 14, pp. 182–183 (1971).
9) Blackwelder, R.F. and Kovasznay, L.S.G.: Time scales and correlation in a turbulent boundary layer, Phys. of Fluids, vol. 15, pp. 1545–1554 (1972).
10) Offen, G.R. and Kline, S.J.: A proposed model of the bursting process in turbulent boundary layers, J. Fluid Mech., vol. 70, pp. 209–228 (1975).
11) Falco, R.E.: Coherent motions in the outer region of turbulent boundary layers, Phys. of Fluids, vol. 20, pp. S124–S132 (1977).
12) Brown, G.L. and Thomas, A.S.W.: Large structure in a turbulent boundary layer, Phys. of Fluids, vol. 20, pp. S243–252 (1977).
13) Praturi, A.K. and Brodkey, R.S.: A stereoscopic visual study of coherent structures in turbulent shear flow, J. Fluid Mech., vol. 89, pp. 251–272 (1978).
14) Grass, A.J.: Structural features of turbulent flow over smooth and rough boundaries, J. Fluid Mech., vol. 50, pp. 233–255 (1971).
15) Jackson, R.E.: Sedimentological and fluid-dynamic implications of the turbulent bursting phenomenon in geophysical flows, J. Fluid Mech., vol. 77, pp. 531–560 (1976).
16) Nakagawa, H. and Nezu, I.: Bursting phenomenon near the wall in open-channel flows and its simple mathematical model, THIS MEMOIRS, Fac. Eng., Kyoto Univ., vol. 40, pp. 213–240 (1978).
17) Nakagawa, H., Nezu, I. and Matsumoto, N.: Structure of space-time correlations of bursting phenomenon in an open-channel flow, THIS MEMOIRS, Fac. Eng., Kyoto Univ., vol. 42, pp. 85–124 (1980). Also, see 3rd Int. Symp. Stochastic Hydraulics, Tokyo, pp. 577–588 (1980).

18) Gupta, A.K., Laufer, J. and Kaplan, R.E.: Spatial structure in the viscous sublayer, J. Fluid Mech., vol. 50, pp. 493–512 (1971).
19) Lu, S.S. and Willmarth, W.W.: Measurements of the structure of the Reynolds stress in a turbulent boundary layer, J. Fluid Mech., vol. 60, pp. 481–511 (1973).
20) Brodkey, R.S., Wallace, J.M. and Eckelmann, H.: Some properties of truncated turbulence signals in bounded shear flows, J. Fluid Mech., vol. 63, pp. 209–224 (1974).
21) Blackwelder, R.F. and Kaplan, R.E.: On the wall structure of the turbulent boundary layer, J. Fluid Mech., vol. 76, pp. 89–112 (1976).
22) Wallace, J.M., Brodkey, R.S. and Eckelmann, H.: Pattern-recognized structures in bounded turbulent shear flows, J. Fluid Mech., vol. 83, pp. 673–693 (1977).
23) Nakagawa, H. and Nezu, I.: Prediction of the contributions to the Reynolds stress from the bursting events in open-channel flows, J. Fluid Mech., vol. 80, pp. 99–128 (1977).
24) Sabot, J. and Comte-Bellot, G.: Intermittency of coherent structures in the core region of fully developed turbulent pipe flow, J. Fluid Mech., vol. 74, pp. 767–796 (1976).
25) Nakagawa, H. and Nezu, I.: Structure of instantaneous Reynolds stress over a permeable open-channel flow with suction or injection, THIS MEMOIRS, Fac. Eng., Kyoto Univ., vol. 41, pp. 240–267 (1979).
26) Utami, T. and Ueno, T.: Study on the structure of large scale turbulence by flow visualizing method (2), Annuals, Dis. Prev. Res. Ins., Kyoto Univ., vol. 20, pp. 331–353 (*in Japanese*).
27) Laufer, J.: The structure of turbulence in fully developed pipe flow, NACA, Technical Report, TR-1174 (1954).
28) Bremhorst, K. and Walker, T.B.: Spectral measurements of turbulent momentum transfer in fully developed pipe flow, J. Fluid Mech., vol. 61, pp. 173–186 (1973).
29) Müller, A.: Effect of secondary flow on turbulence in an open channel, 2nd Int. Symp. Stochastic Hydraulics, No. 3, pp. 1–22 (1977).
30) Kline, S.J., Reynolds, W.C., Schraub, R.A. and Runstadler, P.W.: The structure of turbulent boundary layers, J. Fluid Mech., vol. 30, pp. 741–773 (1967).
31) Nakagawa, H. and Nezu, I.: Visualization of wall turbulence in open-channel flow by hydrogen-bubble method, 5th Symp. Flow Visualization, ISAS, Univ. of Tokyo, No. 5, pp. 47–50 (1977) (*in Japanese*).
32) Nishioka, M., Iida, S. and Shimizu, K.: Three-dimensional structure of turbulence near the wall, 9th Symp. Turbulence, ISAS, Univ. of Tokyo, pp. 129–136 (1977) (*in Japanese*).
33) Lee, M.K., Eckelman, L.D. and Hanratty, T.J.: Identification of turbulent wall eddies through the phase relation of the components of the fluctuating velocity gradient, J. Fluid Mech., vol. 66, pp. 17–33 (1974).
34) Kreplin, H.P. and Eckelmann, H.: Propagation of perturbations in the viscous sublayer and adjacent wall region, J. Fluid Mech., vol. 95, pp. 305–322 (1979).
35) Morrison, W.R.B., Bullock, K.J. and Kronauer, R.E.: Experimental evidence of waves in the sublayer, J. Fluid Mech., vol. 47, pp. 639–656 (1971).
36) Blackwelder, R.F. and Woo, H.H.W.: Pressure perturbation of a turbulent boundary layer, Phys. of Fluids, vol. 17, pp. 515–519 (1974).
37) Fukuoka, S. and Fukushima, Y.: Characteristics of ascending currents and boils induced large-scale eddies, 3rd Int. Symp. Stochastic Hydraulics, Tokyo, pp. 609–619 (1980).
38) Bradshaw, P.: 'Inactive' motion and pressure fluctuations in turbulent boundary layer, J. Fluid Mech., vol. 30, pp. 241–258 (1967).
39) Nakagawa, H. and Nezu, I.: Coherent structures in open-channel flow, Symp. on Heat and Mass Transfer and Structure of Turbulence, Dubrovnik 1980 (to be published soon by Hemisphere Pub. CO.).
40) Nakagawa, H. and Nezu, I.: Structure of space-time correlations of bursting phenomena in an open-channel flow, J. Fluid Mech., vol. 104, pp. 1–43 (1981).